Journal of Power Sources 262 (2014) 349–355

Contents lists available at ScienceDirect

Journal of Power Sources

journal homepage: www.elsevier.com/locate/jpowsour

An investigation on the photoelectrochemical properties of dye-sensitized solar cells based on graphene–TiO_2 composite photoanodes

Menghua Zhu [a], Xin Li [a,b,*], Weiwei Liu [a], Ying Cui [a]

[a] Department of Chemistry, Harbin Institute of Technology, Harbin 150090, China
[b] State Key Lab of Urban Water Resource and Environment, Harbin Institute of Technology, Harbin 150090, China

HIGHLIGHTS

- Graphene–TiO_2 nanocomposites photoanode is prepared.
- 2D graphene bridges exhibits lower charge recombination.
- Performance of DSSCs is enhanced.

GRAPHICAL ABSTRACT

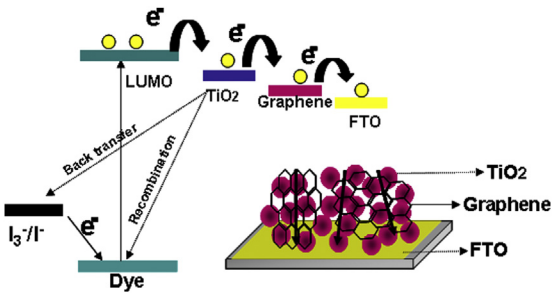

ARTICLE INFO

Article history:
Received 13 December 2013
Received in revised form
12 March 2014
Accepted 2 April 2014
Available online 8 April 2014

Keywords:
Graphene
Titanium dioxide
Photoanode
Dye-sensitized solar cells

ABSTRACT

The graphene–TiO_2 nanocomposite has been prepared by mixing graphene oxide (GO) and tetra-*n*-butyl titanate (TBT) followed by the facile hydrothermal process when the reduction of GO to reduced graphene oxide (RGO) and the hydrolysis of TBT to TiO_2 happen. Characterization of the graphene–TiO_2 nanostructures is investigated in detail by X-ray diffraction, scanning electron microscopy, transmission electron microscopy, and Raman spectroscopy. A dye-sensitized solar cell (DSSC) based on graphene–TiO_2 composite photoelectrode exhibits a high energy conversion efficiency of 4.28%, compared with a DSSC based on pure TiO_2 photoelectrode (3.11%), accompanied by an increment in both short-circuit photocurrent density and open-circuit voltage. The significant enhancement in performance of DSSC is investigated through intensity-modulated photovoltage spectroscopy, intensity-modulated photocurrent spectroscopy, and electrochemical impedance spectroscopy. It is found that the incorporation of two-dimensional graphene nanosheets in the TiO_2 electrodes is the key factor leading to the improved photogenerated electron transfer ability and reduced charge recombination.

1. Introduction

During the past two decades, dye-sensitized solar cells (DSSCs) have gained tremendous interests as a promising alternative to the conventional silicon photovoltaics with an aim of addressing the current energy and environmental crisis [1,2]. DSSCs have many advantages over their counterparts, involving ease of processing, environmental friendliness, low-cost and high energy conversion

* Corresponding author. Department of Chemistry, Harbin Institute of Technology, Harbin 150090, China. Tel.: +86 451 86282153.
E-mail addresses: lixin@hit.edu.cn, lixin_hit@aliyun.com (X. Li).

http://dx.doi.org/10.1016/j.jpowsour.2014.04.001
0378-7753/

efficiency [3,4]. Although up to 12.3% conversion efficiency was achieved [5], even higher light-to-electric efficiency is still a sole goal for the development of DSSCs.

The improvement of conversion efficiency of DSSCs is limited by the photoanode materials; thus an effective approach to enhance the performance of DSSCs is to develop the excellent materials used as photoanode in DSSCs. Since 1991, titanium dioxide (TiO_2), an important semiconductor, has been extensively studied as the most promising photoanode material for DSSCs owing to its superior electrical, optical, and chemical properties [6,7]. In typical TiO_2-based DSSCs, photogenerated electrons transport through mesoporous TiO_2 films to electrode for collection. The high charge-collection efficiency requires fast electron transport to avoid the recombination with the reduced redox species [8–10]. To improve the charge-collection efficiency, one promising solution is to introduce highly electrically conductive carbon materials, such as fullerene [11], carbon nanotubes (CNTs) [12–14], and graphene [15,16] into TiO_2. Amongst various carbon materials, CNTs have been demonstrated to enhance electron transport and thereby improve the performance of DSSCs as one-dimensional (1D) nanomaterials. CNTs in DSSCs offer an electron transport superhighway [14] due to the formation of 1D CNTs bridges between TiO_2 nanoparticles of photoanode [12]. However, the main drawback of 1D bridge is the poor point contact between TiO_2 and CNTs, leading to low electron transport and decrease in the efficiency of the DSSCs [15]. To address this issue, Incorporation grapheme with TiO_2 matrix may be expected to improve the electron transport across the mesoporous film.

Graphene, a novel two-dimensional (2D) nanomaterial with one-atom thickness, exhibits low resistance, excellent optical transmittance and electron transport [17–19]. As a result of its high mobility up to 10^6 cm^2 V^{-1} s^{-1} [20], high specific surface area reaching 2630 m^2 g^{-1} [21], tunable band gap, and high mechanical strength, graphene should be an ideal material in DSSC photoanodes. To date, there have been a few reports on the enhancement of DSSCs by using graphene–TiO_2 composites as photoanode materials. For examples, Sun et al. reported the effectively enhance the performance of DSSCs by using graphene/P25 photoanode prepared by heterogeneous coagulation [22]. Tang et al. introduced graphene sheets in TiO_2 films through an *in situ* molecular grafting method, their results indicated significantly increases photocurrent through DSSCs [23]. Song et al. demonstrated the enhancement of photocurrent, fill factor, and the overall conversion efficiency of DSSCs due the forming of reduced graphene oxide (RGO)–TiO_2 Schottky barrier junction [24]. Zhu et al. incorporated graphene in TiO_2 photoanode, thus improved the performance of quantum dot-sensitized solar cells [25]. Madhavan et al. reported the electrospinning of TiO_2–graphene composite nanofibers as photoanodes in DSSCs [26]. Tang and Hu showed that graphene modified TiO_2 composites have great light-harvesting efficiencies [27]. Chen et al. proposed a novel method to enhance the power conversion efficiency *via* graphene functionalization of fluorinated-tin oxide surface [28]. Very recently, Chen et al. reported an enhanced photovoltaic performance of a DSSC using graphene–TiO_2 photoelectrodes prepared by simultaneous reduction-hydrolysis approach [29]. Hu and co-workers have found that the three-dimensional (3D) graphene network boost the photovoltaic performance of DSSCs [30]. Cheng et al. reported an improved overall light-to-electricity conversion efficiency from 4.78% to 7.68% when RGO was incorporated into the device [31]. Wu and co-workers mixed colloid of graphene and titania to prepare photoanode, thus improved the photovoltaic performance of quantum dots-sensitized solar cell [32]. Shu et al. obtained the best conversion efficiency of 5.5% using RGO–TiO_2 nanocrystals composite photoanode [33]. More recently, Tan's group reported high performance DSSCs using graphene–TiO_2 nanocomposites as photoanode materials [34,35]. Despite the above progress, the role of graphene and the mechanisms of graphene-based photoanode materials remain unclear. Jiang and co-workers have recently suggested that the 2D graphene bridges can provide pathways for a faster electron transport and lower recombination in DSSCs [36]. In view of this, further systematic investigations are highly desired for improving photovoltaic performance of DSSCs.

In the present work, we describe the incorporation of 2D graphene sheets into TiO_2 nanoparticle photoanodes using one-step hydrothermal approach. A high power conversion efficiency of 4.28% in DSSCs was achieved. Electrochemical impedance spectroscopy (EIS), intensity-modulated photovoltage spectroscopy (IMVS), and intensity-modulated photocurrent spectroscopy (IMPS) measurements clearly indicate efficient charge transport and recombination suppression on graphene–TiO_2 hybrids.

2. Experimental

2.1. Reagents and materials

Tetrabutyl titanate, chloroplatinic acid, iodine, lithium iodide, diacetylmethane, ethyl cellulose (EC), terpineol and N719 dye were purchased from the Aladdin. Fluorine-doped tin oxide (FTO) conducting glass plates (sheet resistance 10 Ω sq^{-1}) were purchased from Qiseguang Technology Ltd. in China.

2.2. Hydrothermal synthesis of graphene–TiO_2 hybrids

Graphene oxide (GO) was prepared by the modified Hummers method [37].

The design of a graphene–TiO_2 hybrid is a work inspired by He's report [34]. In a typical process, 1 ml tetrabutyl titanate was first added into 10 ml mixed solution (8 ml ethanol and 2 ml acetic acid) during strong stirring process. After stirring for 30 min, 20 ml deionized water was then added into the mixed solution. Subsequently, 0.04 g GO was dispersed in 5 ml of ethanol: deionized water (1:1 volume ratio) by sonication for 30 min, and the GO solution was then dropped into the above tetrabutyl titanate solution. The mixture was refluxed at 80 °C for 2 h. After mixing with 17 ml NaOH (10 mol L^{-1}), the obtained solution was transferred to a Teflon-lined container with a sealed iron shell and heated at 180 °C for 20 h. Finally, the resulting products were collected by filtration, washing/centrifugation, and dried for 3 h at 80 °C.

As a reference, TiO_2 nanoparticles, which did not contain the GO, were also prepared in the same synthetic condition.

2.3. Preparation of TiO_2 paste and graphene–TiO_2 paste

2.00 g As-prepared graphene–TiO_2 hybrids or (TiO_2 nanoparticles) was first suspended in 50 ml absolute ethanol, and stirred at room temperature for 2 h and sonicated for 1 h. 1.00 g EC powder was then dissolved in 50 ml absolute ethanol, and mixed with TiO_2 nanoparticles suspension, followed by sonication for 1 h at 60 °C. Terpineol (8 ml) was added dropwise into the as-prepared mixture. Subsequently, the ethanol in the mixture was removed on a rotary-evaporator at 40 °C.

2.4. Fabrication of DSSCs

Graphene–TiO_2 (or TiO_2) films (8.0 μm) were screen-printed on FTO substrate, followed by being sintered at 450 °C for 1 h and 500 °C for 15 min in nitrogen. After cooling down to 80 °C, the sintered photoanodes were immersed in 0.5 mM N719 dye in acetonitrile/*tert*-butanol mixed solution (1:1, v/v) for 24 h. The platinized counter electrodes were prepared by thermal deposition

of H_2PtCl_6 solution (5 M in isopropanol) onto FTO glass at 400 °C for 30 min.

The iodide/triiodide electrolyte contains 0.60 M 1-methyl-3-propylimidazolium iodide (PMII), 0.10 M guanidinium thiocyanate, 0.03 M I_2, 0.50 M *tert*-butylpyridine (TBP) dissolved in an acetonitrile/valeronitrile mixture (85:15, v/v).

2.5. Characterization and measurements

Scanning electron microscopic (SEM) images were taken with a Zeiss Supra 40 FE SEM. Transmission electron microscopy (TEM) experiment was performed on an electron microscope (H-7650, Japan) with an acceleration voltage of 80 kV. X-ray diffraction (XRD) analysis was recorded on a XRD-6000 X-ray diffractometer (Shimadzu) with Cu Kα radiation ($\lambda = 1.5406$ Å). Raman spectrometers were characterized by Jobin Yvon HR 800.

Photocurrent density–voltage (J–V) curves were measured with an electrochemical workstation (BAS100B electrochemical analyzer, Bioanalytical Systems Inc., USA) under AM1.5 radiation (1 sun conditions, 100 mW cm^{-2}). IMPS and IMVS (Zahner Elektrik, Germany) were performed with a frequency response analyzer using a white light emitting diode (wlr-01) as the light source. The EIS were performed with an EC-Lab impedance device unit and obtained by under AM1.5 radiation at a frequency range of 0.01 Hz–100 kHz.

3. Results and discussion

3.1. Characterization of graphene–TiO_2 hybrids

XRD characterization was conducted to determine the crystal structural about TiO_2 and graphene–TiO_2, and the results are shown in Fig. 1a. As displayed in Fig. 1a, the diffraction peaks can be well indexed to the (101), (004), 112, (200), (105), (211), and (204) crystal planes of anatase TiO_2 (JCPDS 19-0629). Furthermore, the characteristic peaks of graphene was not effectively detected due to the smaller content of graphene in the hybrid, which was also observed in the reported literature [32,33]. The observation of XRD confirms the presence anatase TiO_2 in the graphene–TiO_2.

Raman spectroscopy is a sensitive analytical tool to characterize structure properties of graphitic materials. Raman spectroscopy was employed to analyze GO and graphene–TiO_2. As shown in Fig. 1b, the Raman spectra of GO exhibited a D (disorder) peak at 1333 $cm^{-1}$and a G (graphitic) peak at 1580 cm^{-1} [38]. It is well known that the intensity ratio of D band to G band (I_D/I_G) corresponds to the in-plane crystallite dimension and is a main feature of disorder in the material [39]. In our case, the I_D/I_G was 1.28 for graphene–TiO_2, and it increased compared to that of the GO ($I_D/I_G = 1.15$), which suggests the increase in disorder and confirms the occurrence of graphene functionalization [40,41]. The Raman spectroscopy analysis further reveals the successful preparation of graphene–TiO_2 by using one-step hydrothermal reaction.

The morphological characteristics of the as-synthesized TiO_2 and graphene–TiO_2 were characterized by SEM, TEM, and high-resolution TEM (HRTEM). As seen from Fig. 2, the TiO_2 nanoparticles possess rough surface (Fig. 2a), and the graphene was successfully coated by TiO_2 nanoparticles (Fig. 2b). It can be seen from Fig. 2b that the graphene–TiO_2 composites have good contact between graphene sheets and TiO_2 nanoparticles, which facilitate the electron transfer from TiO_2 to graphene. The TEM image (Fig. 3a) displays that the TiO_2 nanoparticles with diameters of 7–15 nm homogeneously spread on the surface of graphene. Additionally, the HRTEM image (Fig. 3b) indicates the high crystallinity

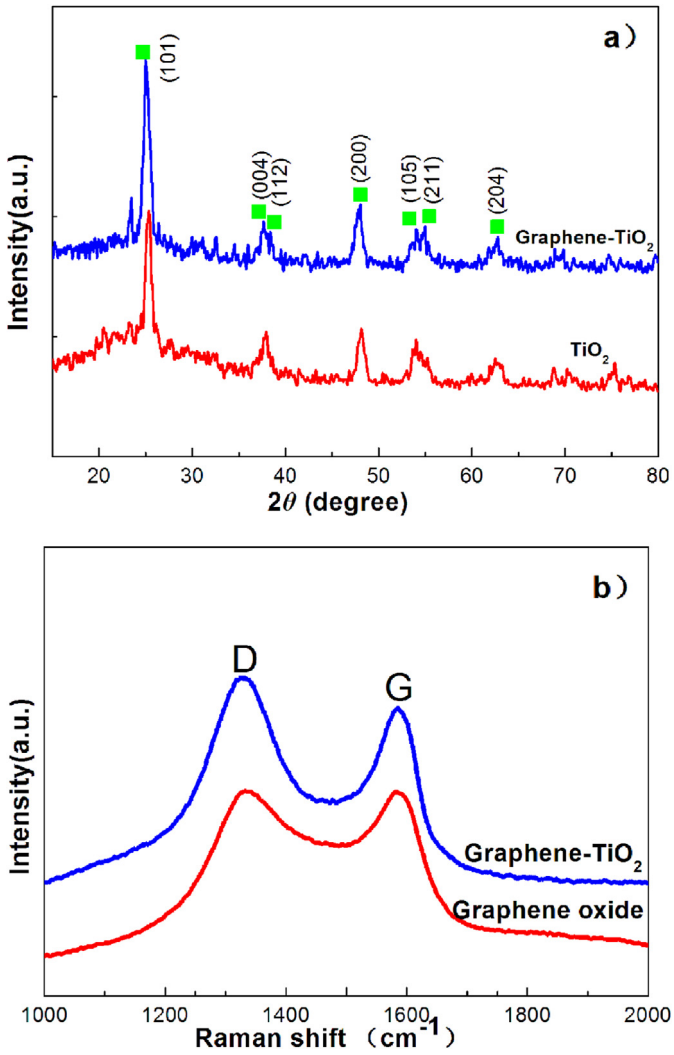

Fig. 1. XRD patterns of TiO_2 and graphene–TiO_2 (a); Raman spectra of graphene oxide and graphene–TiO_2 (b).

of the nanoparticles with lattice spacings of 0.35 nm, corresponding to (101) plane of the anatase TiO_2, which is consistent with the XRD analysis. Obviously, the graphene–TiO_2 composite structures have been formed.

3.2. Photovoltaic characteristics of DSSCs

The J–V curves of the assembled DSSCs with the TiO_2 and graphene–TiO_2 photoanodes are shown in Fig. 4, and the corresponding performance parameters of the DSSCs are summarized in Table 1. DSSCs with TiO_2 photoanode exhibit an open-circuit voltage (V_{oc}) of 0.66 V and short-circuit current density (J_{sc}) of 7.85 mA cm^{-2}, yielding conversion efficiency (η) of 3.11%. Interestingly, the performances of DSSCs are greatly improved by using graphene–TiO_2 photoanode. A higher η of 4.28% with V_{oc} of 0.75 V and J_{sc} of 10.07 mA cm^{-2} are observed, and the increases for the η and J_{sc} reach 38% and 28%, respectively. It is worth to note that the DSSC fabricated with the graphene–TiO_2 photoanode had a higher V_{oc} than that of the DSSC fabricated with the TiO_2 photoanode, indicating that the enhancement of η is responsible for the both higher J_{sc} and V_{oc}. This increment in η could be attributed to the effect of graphene. Generally, the V_{oc} is expressed by Equation (1) [33,42,43]:

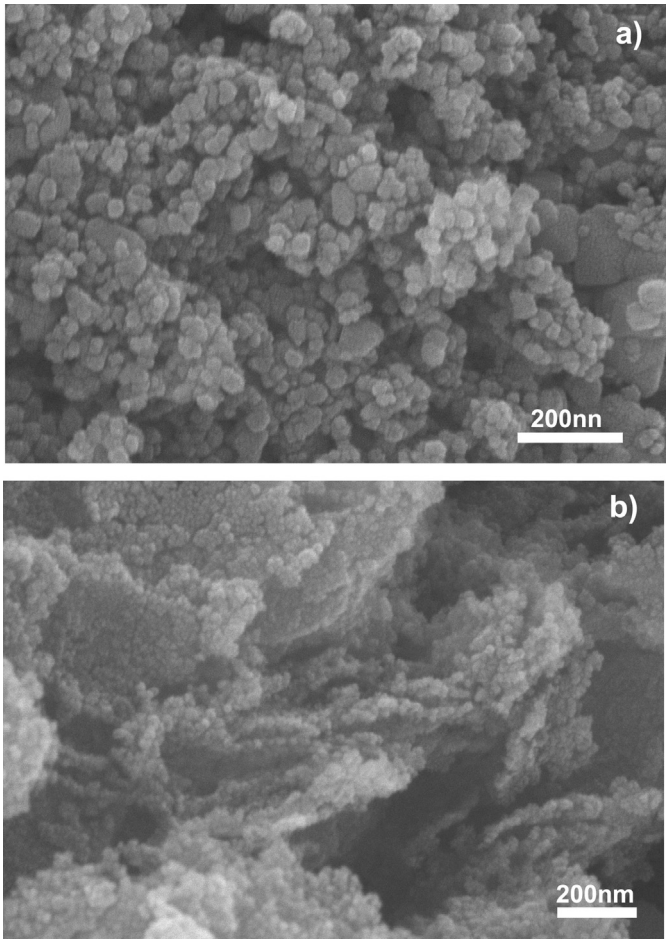

Fig. 2. SEM micrographs of TiO_2 (a) and graphene–TiO_2 (b).

$$V_{oc} = \varepsilon_{redox} - \varepsilon_c - \frac{\gamma \kappa_B T}{e} \ln\left(\frac{N_e}{n}\right) \quad (1)$$

where N_e is the effective density of states at the TiO_2 conduction band edge, ε_{redox} is electrolytic redox level, ε_c is conduction band edge level of TiO_2, γ is characteristic constant of TiO_2 tailing states, $\boldsymbol{k}_B$ is the Boltzmann constant, T is temperature, and e is the elementary charge.

Equation (1) indicates that V_{oc} is mainly determined by the apparent Fermi level and electron density (n) in TiO_2 conduction band (CB), and in turn, it is directly depend on the surface charge and charge recombination at the TiO_2/electrolyte interface [44–46]. When incorporation of 2D graphene nanosheets in the TiO_2 electrodes of DSSCs, the graphene bridges would provide an improved photogenerated electron transfer ability and reduced charge recombination, and the higher electron density in TiO_2 CB will result in increasing open circuit voltage. Similar behaviors have been reported to DSSCs with graphene–TiO_2 photoanodes [34,46,47]. For the J_{sc}, an increase in J_{sc} could be related to the high dye loading capacity arising from the ultrahigh surface area of graphene [48].

EIS measurement was further performed to confirm the effect of graphene on improving photovoltaic performance of DSSCs. Fig. 5 shows the Nyquist plots of DSSCs fabricated with TiO_2 and graphene–TiO_2 photoanodes under AM1.5 radiation. In the Nyquist plots, two typically semicircles in the high-frequency (kHz) and medium-frequency (1–100 Hz) were observed in both curves. The no obvious small semicircle in the high-frequency region corresponds to the redox reaction at I^-/I_3^-/Pt counter-electrode interface, and the large semicircle in the medium-frequency region relates to the electron transfer at the photoanode–electrolyte interface [49–51]. According to the previous study [38], the radius of arc in the medium-frequency region reflects charge transfer ability. Fig. 5 clearly showed that the semicircle size for the graphene–TiO_2 photoanode in the medium-frequency region exhibits significant reduction than that for the TiO_2 photoanode, reflecting faster electron transfer process and lower charge recombination due to the effective photogenerated electron separation and transport through the 2D graphene bridges.

A transmission line model, shown in Fig. 5, is used to characterize the measured EIS of DSSCs based on TiO_2 and graphene–TiO_2, aimed at simultaneously estimating the recombination resistance (R_r) and transport resistance (R_t) in the porous TiO_2 network. [52–54] The diffusion-recombination model [55] and continuity equations [56] proposed by Bisquert and Kern for describing the impedance models of DSSCs, respectively, were proved to be derived to the same equation by Adachi [57]. This model can be expressed as following formula without considering the effects of the Pt electrode or the diffusion in the electrolyte,

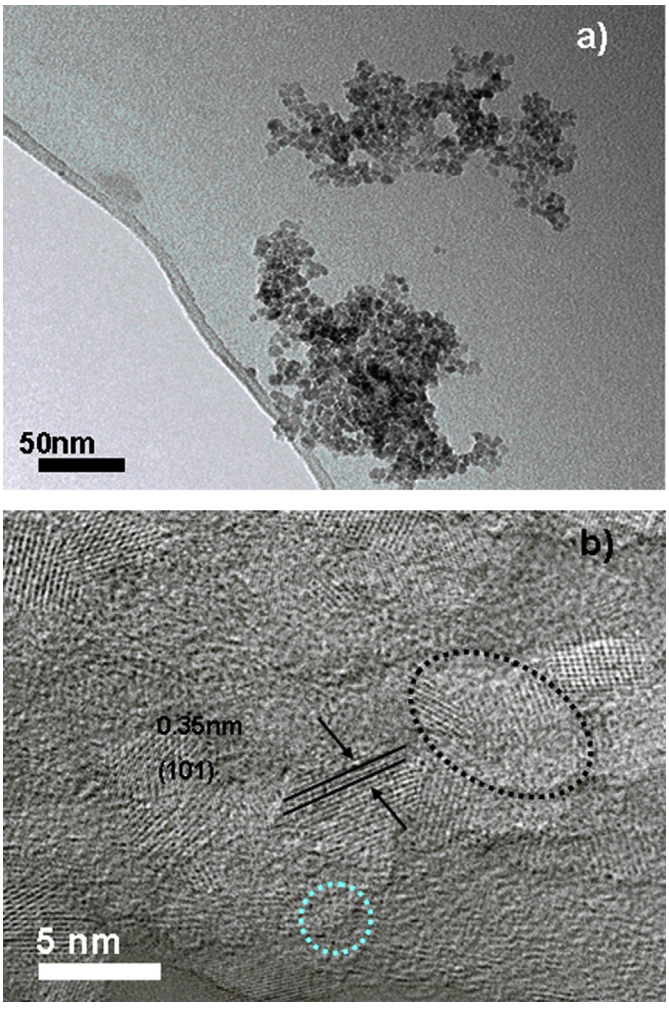

Fig. 3. TEM (a) and HRTEM (b) images of graphene–TiO_2.

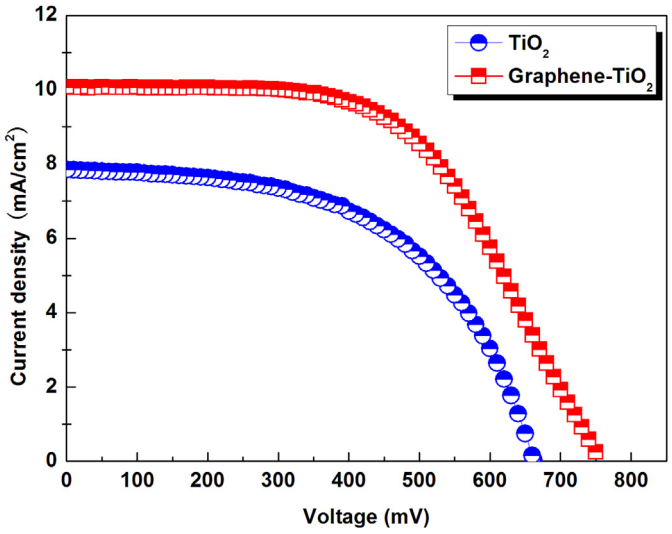

Fig. 4. J–V characteristics of DSSCs based on TiO_2 and graphene–TiO_2 photoelectrodes under illumination with light intensity of 100 mW cm^{-2}.

Table 1
Photovoltaic parameters for DSSCs based on TiO_2 and graphene–TiO_2 anodic materials under 100 mW cm^{-2} illumination.

Sample	V_{oc} (mV)	J_{sc} (mA cm^{-2})	FF	η (%)
TiO_2	660	7.85	0.60	3.11
Graphene–TiO_2	753	10.07	0.57	4.28

$$Z = \left(\frac{R_t R_r}{1 + i\omega/\omega_k}\right)^{\frac{1}{2}} \coth\left[\left(\frac{\omega_k}{\omega_d}\right)^{\frac{1}{2}}\left(1 + \frac{i\omega}{\omega_k}\right)\right]^{\frac{1}{2}} \quad (2)$$

where R_t and R_r are recombination and transport resistance, respectively. $\omega_d = 1/R_t C_\mu$ and $\omega_k = 1/R_r C_\mu$ represent characteristics transport and recombination frequency, respectively. C_μ is the chemical capacitance. ω is the angular frequency.

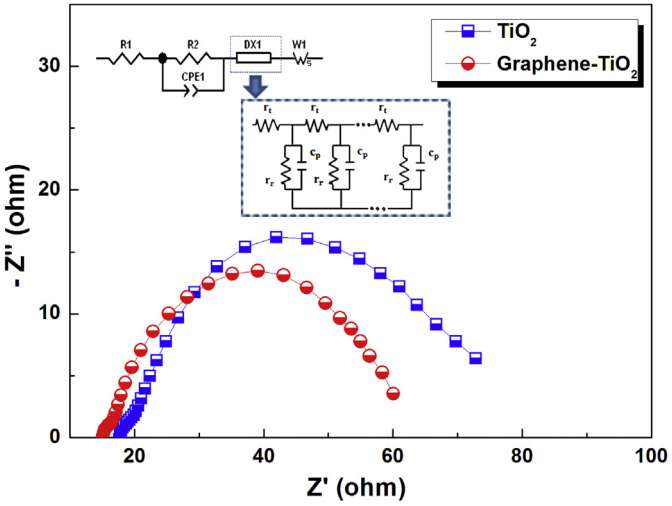

Fig. 5. Nyquist diagrams of DSSCs with TiO_2 and graphene–TiO_2 electrode under AM1.5 radiation. The inset is equivalent circuit model for fitting Nyquist plot. R1 represents series resistance, R2 represents resistance of counter electrode, CPE1 represents double layer capacitance of counter electrode, and W1 (Ws) represents Warburg impedance. DX1 is complicated elements in the equivalent circuit model.

Taking into account the electron transfer at Pt/electrolyte and electrolyte diffusion, a full equivalent circuit model of a DSSC was presented in Fig. 5 (inset in Fig. 5). The element units in the equivalent circuit model are explained in Fig. 5, corresponding to the transmission line model. Of note, DX1 is complicated element in the equivalent circuit model (DX type TL-Open, in Zview) [58]. Therefore, the parameters in Equation (2), including R_r, R_t and C_μ, could be simultaneously obtained by fitting Nyquist plot using Zview software and corresponding EIS parameters are summarized in Table 2. For the DSSC with graphene–TiO_2 photoanode, the recombination resistance (R_r) is 35.27 Ω, 1.18 times higher than that of DSSC with TiO_2 photoanode (29.82 Ω), indicating lower recombination of charge and higher V_{oc} of DSSC [59,60]. As expected, the electron transport resistance (R_t) for graphene–TiO_2 photoanode is significantly reduced to 6.730 Ω, compared with that of TiO_2 photoanode (19.032 Ω). Meanwhile, the chemical capacitance increases form 11.318 μF for TiO_2 photoanode to 13.961 μF for graphene–TiO_2 photoanode. A lower transport resistance leads to a faster interfacial charge transfer process, and higher chemical capacitance indicates increased dye adsorption [34], may give the high η. These results are in agreement with the J–V behavior as discussed above.

To further understand the effect of graphene on performance of the DSSCs, IMPS/IMVS measurements were carried out to investigate the dynamics of electron recombination and transport under illumination. The electron recombination time (τ_r) and the electron transport time (τ_t) are calculated using the following expression:

$$\tau_r = \frac{1}{2\pi f_r} \quad (3)$$

$$\tau_t = \frac{1}{2\pi f_t} \quad (4)$$

where f_r (f_t) is the characteristic frequency minima of the IMVS (IMPS) imaginary component [61].

As shown in Fig. 6a, the IMVS shows that the electron recombination time of the graphene-based DSSC is longer than that of the TiO_2-based DSSC. Meanwhile, IMPS indicates that electron transport time is greatly reduced for graphene–TiO_2 photoanode (Fig. 6b). The longer recombination time and shorter transport time for graphene–TiO_2 photoanode are attributed to the graphene bridges as discussed above. The obtained results are consistent with the EIS analysis shown above. Furthermore, the recombination time and transport time of the both DSSCs exponential decrease with increasing light intensity, which relate to the trap-limited transport [62]. This is because the light intensity dependent is related to the trap state distribution, and thus changes the electron recombination probability.

It is well known that the charge collection efficiency (η_{cc}) and the electron diffusion length (L_n) are important parameters to estimate the performance of DSSCs. These parameters, as reliable index, are determined by the competition between the electron transport and recombination. Both η_{cc} and L_n values can be

Table 2
Detailed EIS parameters for the DSSCs with TiO_2 and graphene–TiO_2 photoelectrodes.

Sample	R_{cr} (Ω)	R_t (Ω)	C (F)
TiO_2	29.82	19.032	1.1318×10^{-5}
Graphene + TiO_2	35.27	6.730	1.3961×10^{-5}

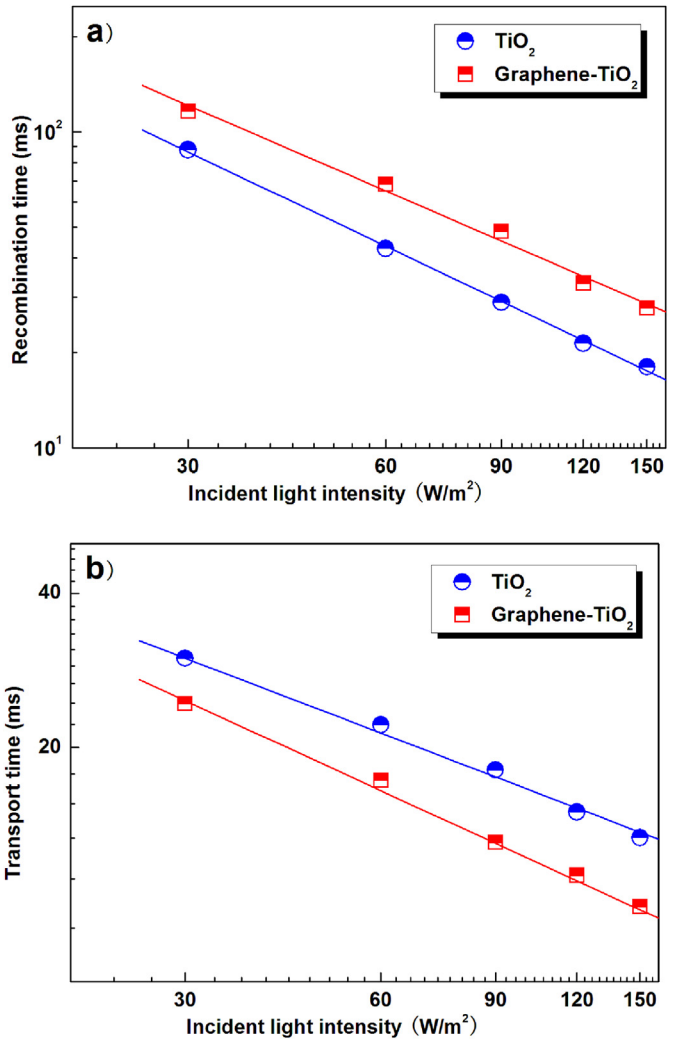

Fig. 6. The IMVS response (a) and IMPS response (b) of DSSCs based on TiO_2 and graphene–TiO_2 photoelectrodes.

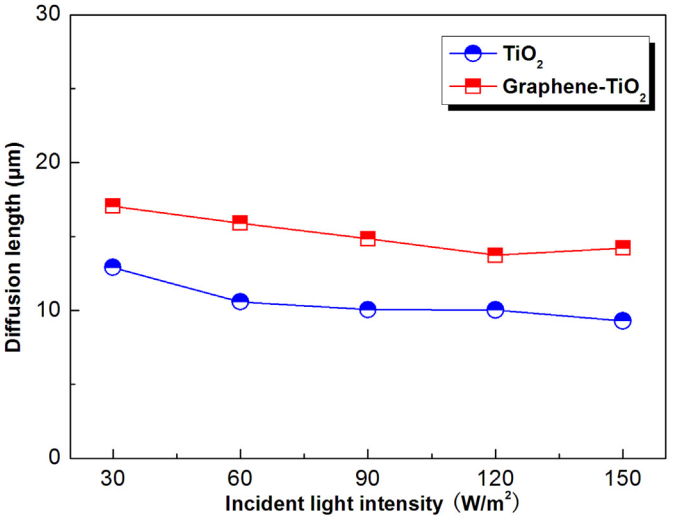

Fig. 7. Electron diffusion length of DSSCs based on TiO_2 and graphene–TiO_2 photoelectrodes.

calculated by IMPS/IMVS measurements according to the expression:

$$\eta_{cc} = 1 - \frac{\tau_t}{\tau_r} \tag{5}$$

$$L_n = \left(L^2 \frac{\tau_r}{\tau_t}\right)^{\frac{1}{2}} \tag{6}$$

where L is the photoelectrode thickness.

According to Equation (5), η_{cc} value for graphene-based DSSC is calculated to be 78% at a constant light intensity (90 W m^{-2}), which is 20% larger than that for TiO_2-based DSSC (65%). From examining the calculated L_n values presented in Fig. 7, a longer L_n was found in graphene-based DSSC. A high η_{cc} and L_n were found in graphene-based DSSC suggest the electron recombination suppression in graphene–TiO_2 photoanode and a higher converse efficiency for DSSC.

4. Conclusions

In conclusion, we have successfully prepared graphene–TiO_2 nanocomposites through a simple one-step solvothermal approach. Compared with that of a DSSC based on pure TiO_2 photoelectrode, the energy conversion efficiency for a DSSC based on graphene–TiO_2 photoelectrode increase by 38%. This increase is attributed to the effect of graphene, 2D charge transfer bridges, leading to the improved photogenerated electron transfer ability and reduced charge recombination.

Acknowledgments

We are grateful for the financial support from the National Natural Science Foundation of China (No. 21176052), Specialized Research Fund for the Doctoral Program of Higher Education (20122302110043), the State Key Laboratory of Urban Water Resource and Environment, Harbin Institute of Technology (2013TS05), and Program for Innovation Research of Science in Harbin Institute of Technology.

References

[1] B. Oregan, M. Grätzel, Nature 353 (1991) 737.
[2] M. Grätzel, Acc. Chem. Res. 42 (2009) 1788.
[3] J. Gong, J. Liang, K. Sumathy, Renew. Sustain. Energy Rev. 16 (2012) 5848.
[4] S. Zhang, X. Yang, Y. Numata, L. Han, Energy Environ. Sci. 6 (2013) 1443.
[5] A. Yella, H.W. Lee, H.N. Tsao, C. Yi, A.K. Chandiran, M.K. Nazeeruddin, E.W.G. Diau, C.Y. Y eh, S.M. Zakeeruddin, M. Grätzel, Science 334 (2011) 629.
[6] A.L. Linsebigler, G. Lu, J.T.J. Yates, Chem. Rev. 95 (1995) 735.
[7] M. Adachi, R. Tanino, J. Adachi, Y. Mori, K. Tsuchiya, S. Isoda, F. Uchida, J. Power Sources 226 (2013) 94.
[8] K. Zhu, N.R. Neale, A. Miedaner, A.J. Frank, Nano Lett. 7 (2007) 69.
[9] M.Y. Yen, M.C. Hsiao, S.H. Liao, P.I. Liu, H.M. Tsai, C.C.M. Ma, N.W. Pu, M.D. Ger, Carbon 49 (2011) 3597.
[10] Y.C. Lin, Y.T. Chen, P.C. Yao, J. Power Sources 240 (2013) 705.
[11] T. Hasobe, S. Hattori, P.V. Kamat, Y. Urano, N. Umezawa, T. Nagano, S. Fukuzumi, Chem. Phys. 319 (2005) 243.
[12] A. Kongkanand, R.M. Dominguez, P.V. Kamat, Nano Lett. 7 (2007) 676.
[13] Y. Yao, G. Li, S. Ciston, R.M. Lueptow, K.A. Gray, Environ. Sci. Technol. 42 (2008) 4952.
[14] L. Yang, W.W.F. Leung, Adv. Mater. 25 (2013) 1792.
[15] L.J. Brennan, M.T. Byrne, M. Bari, Y.K. Gun'ko, Adv. Energy Mater. 1 (2011) 472.
[16] D. Chen, H. Zhang, Y. Liu, J. Li, Energy Environ. Sci. 6 (2013) 1362.
[17] A.K. Geim, K.S. Novoselov, Nat. Mater. 6 (2007) 183.
[18] Y. Sun, Q. Wu, G. Shi, Energy Environ. Sci. 4 (2011) 1113.
[19] A.K. Geim, Science 324 (2009) 1530.
[20] F. Bonaccorso, Z. Sun, T. Hasan, A.C. Ferrari, Nat. Photonics 4 (2010) 611.
[21] A.A. Balandin, S. Ghosh, W. Bao, I. Calizo, D. Teweldebrhan, F. Miao, C.N. Lau, Nano Lett. 8 (2008) 902.
[22] S. Sun, L. Gao, Y. Liu, Appl. Phys. Lett. 96 (2010) 083113.

[23] Y.B. Tang, C.S. Lee, J. Xu, Z.T. Liu, Z.H. Chen, Z.B. He, Y.L. Cao, G.D. Yuan, H.S. Song, L.M. Chen, L.B. Luo, H.M. Cheng, W.J. Zhang, I. Bello, S.T. Lee, ACS Nano 4 (2010) 3482.
[24] J.L. Song, Z.Y. Yin, Z.J. Yang, P. Amaladass, S.X. Wu, J. Ye, Y. Zhao, W.Q. Deng, H. Zhang, X.W. Liu, Chem. Eur. J. 17 (2011) 10832.
[25] G. Zhu, T. Xu, T. Lv, L.K. Pan, Q.F. Zhao, Z. Sun, J. Electroanal. Chem. 650 (2011) 248.
[26] A.A. Madhavan, S. Kalluri, D.K. Chacko, T.A. Arun, S. Nagarajan, K.R.V. Subramanian, A.S. Nair, S.V. Nair, A. Balakrishnan, RSC Adv. 2 (2012) 13032.
[27] B. Tang, G. Hu, J. Power Sources 220 (2012) 95.
[28] T. Chen, W. Hu, J. Song, G.H. Guai, C.M. Li, Adv. Funct. Mater. 22 (2012) 5245.
[29] L. Chen, Y. Zhou, W. Tu, Z. Li, C. Bao, H. Dai, T. Yu, J. Liu, Z. Zou, Nanoscale 5 (2013) 3481.
[30] B. Tang, G. Hu, H. Gao, Z. Shi, J. Power Sources 234 (2013) 60.
[31] G. Cheng, M.S. Akhtar, O.B. Yang, F.J. Stadler, ACS Appl. Mater. Interfaces 5 (2013) 6635.
[32] J. Zhao, J. Wu, F. Yu, X. Zhang, Z. Lan, J. Lin, Electrochim. Acta 96 (2013) 110.
[33] W. Shu, Y. Liu, Z. Peng, K. Chen, C. Zhang, W. Chen, J. Alloys Compd. 563 (2013) 229.
[34] Z. He, G. Guai, J. Liu, C. Guo, J.S.C. Loo, C.M. Li, T.T.Y. Tan, Nanoscale 3 (2011) 4613.
[35] Z. He, H. Phan, J. Liu, T.Q. Nguyen, T.T.Y. Tan, *Adv. Mater.* 25 (2013) 6900.
[36] N. Yang, J. Zhai, D. Wang, Y. Chen, L. Jiang, ACS Nano 4 (2010) 887.
[37] W.S. Hummers, R.E. Offeman, J. Am. Chem. Soc. 80 (1958) 1339.
[38] N.J. Bell, Y.H. Ng, A. Du, H. Coster, S.C. Smith, R. Amal, J. Phys. Chem. C 115 (2011) 6004.
[39] K.N. Kudin, B. Ozbas, H.C. Schniepp, R.K. Prud'homme, I.A. Aksay, R. Car, Nano Lett. 8 (2008) 36.
[40] A.K. Manna, S.K. Pati, Chem. Asian J. 4 (2009) 855.
[41] J. Shen, Y. Hu, M. Shi, N. Li, H. Ma, M. Ye, J. Phys. Chem. C 114 (2010) 1498.
[42] A. Usami, S. Seki, Y. Mita, H. Kobayashi, H. Miyashiro, N. Terada, Sol. Energy Mater. Sol. C 93 (2009) 840.
[43] B.J. Song, H.M. Song, I.T. Choi, S.K. Kim, K.D. Seo, M.S. Kang, M.J. Lee, D.W. Cho, M.J. Ju, H.K. Kim, Chem. Eur. J. 17 (2011) 11115.
[44] Z. Zhang, N. Evans, S.M. Zakeeruddin, R. Humphry-Baker, M. Grätzel, J. Phys. Chem. C 111 (2007) 398.
[45] H. Yang, G.H. Guai, C. Guo, Q. Song, S.P. Jiang, Y. Wang, W. Zhang, C.M. Li, J. Phys. Chem. C 115 (2011) 12209.
[46] T.H. Tsai, S.C. Chiou, S.M. Chen, Int. J. Electrochem. Sci. 6 (2011) 3333.
[47] G.D. Sharm, D. Daphnom ili, K.S.V. Gupta, T. Gayathri, S.P. Singh, P.A. Angaridis, T.N. Kitsopoulos, D. Tasis, A.G. Coutsolelos, RSC Adv. 3 (2013) 22412.
[48] Y.H. Jang, X. Xin, M. Byun, Y.J. Jang, Z. Lin, D.H. Kim, Nano Lett. 12 (2012) 479.
[49] Q. Wang, J.E. Moser, M. Grätzel, J. Phys. Chem. B 109 (2005) 14945.
[50] G. Zhang, K. Pan, W. Zhou, Y. Qu, Q. Pan, B. Jiang, G. Tian, G. Wang, Y. Xie, Y. Dong, X. Miao, C. Tian, Dalton Trans. 41 (2012) 12683.
[51] K. Pan, Y. Dong, W. Zhou, G. Wang, Q. Pan, Y. Yuan, X. Miao, G. Tian, Electrochim. Acta 88 (2013) 263.
[52] F. Fabregat-Santiago, G. Garcia-Belmonte, J. Bisquert, A. Zaban, P. Salvador, J. Phys. Chem. B 106 (2002) 334.
[53] J. Bisquert, G. Garcia-Belmonte, F. Fabregat-Santiago, N.S. Ferriols, P. Bogdanoff, E.C. Pereira, J. Phys. Chem. B 104 (2000) 2287.
[54] A. Pitarch, G. Garcia-Belmonte, I. Mora-Seró, J. Bisquert, Phys. Chem. Chem. Phys. 6 (2004) 2983.
[55] J. Bisquert, J. Phys. Chem. B 106 (2002) 325.
[56] R. Kern, R. Sastrawan, J. Ferber, R. Stangl, J. Luther, Electrochim. Acta 47 (2002) 4213.
[57] M. Adachi, M. Sakamoto, J. Jiu, Y. Ogata, S. Isoda, J. Phys. Chem. B 110 (2006) 13872.
[58] J. Qiu, F. Zhuge, K. Lou, X. Li, X. Gao, X. Gan, W. Yu, H.K. Kim, Yoon H. Hwang, J. Mater. Chem. 21 (2011) 5062.
[59] Y.F. Chan, C.C. Wang, B.H. Chen, C.Y. Chen, Prog. Photovolt. Res. Appl. 21 (2013) 47.
[60] W. Yuan, H. Zhao, H. Hu, S. Wang, G.L. Baker, ACS Appl. Mater. Interfaces 5 (2013) 4155.
[61] X. Miao, K. Pan, Y. Liao, W. Zhou, Q. Pan, G. Tian, G. Wang, J. Mater. Chem. A 1 (2013) 9853.
[62] M. Zhong, J. Shi, W. Zhang, H. Han, C. Li, Mater. Sci. Eng. B Adv. 176 (2011) 1115.